International Journal of Nanomedicine

Dovepress

open access to scientific and medical research

Open Access Full Text Article

ORIGINAL RESEARCH

Huperzine A-Liposomes Efficiently Improve Neural Injury in the Hippocampus of Mice with Chronic Intermittent Hypoxia

Xin-Yue Yang[1,*], Lina Geng[2,*], Ronghui Li[2], Ji-Xian Song[1], Cui-Ling Jia[1], Ji-Ren An[1,3], Meng-Fan Sun[1], Shan Xu[1], Ya-Jing Guo[1], Yashuo Zhao[1], En-Sheng Ji[1]

[1]Hebei Technology Innovation Center of TCM Combined Hydrogen Medicine, Hebei University of Chinese Medicine, Shijiazhuang, People's Republic of China; [2]College of Chemistry and Material Science, Hebei Normal University, Shijiazhuang, People's Republic of China; [3]The First Clinical College, Liaoning University of Traditional Chinese Medicine, Shenyang, People's Republic of China

*These authors contributed equally to this work

Correspondence: Yashuo Zhao; En-Sheng Ji, No. 3, Luqian Xingyuan Road, Shijiazhuang, 050200, People's Republic of China, Email zys870207@126.com; jesphy@126.com

Background: Chronic intermittent hypoxia (CIH) could cause neuronal damage, accelerating the progression of dementia. However, safe and effective therapeutic drugs and delivery are needed for successful CIH therapy.

Purpose: To investigate the neuroprotective effect of Huperzine A (HuA) packaged with nanoliposomes (HuA-LIP) on neuronal damage induced by CIH.

Methods: The stability and release of HuA-LIP in vitro were identified. Mice were randomly divided into the Control, CIH, HuA-LIP, and HuA groups. The mice in the HuA and HuA-LIP groups received HuA (0.1 mg/kg, i.p.), and HuA-LIP was administered during CIH exposure for 21 days. HuA-LIP contains the equivalent content of HuA.

Results: We prepared a novel formulation of HuA-LIP that had good stability and controlled release. First, HuA-LIP significantly ameliorated cognitive dysfunction and neuronal damage in CIH mice. Second, HuA-LIP elevated T-SOD and GSH-Px abilities and decreased MDA content to resist oxidative stress damage induced by CIH. Furthermore, HuA-LIP reduced brain iron levels by downregulating TfR1, hepcidin, and FTL expression. In addition, HuA-LIP activated the PKAα/Erk/CREB/BDNF signaling pathway and elevated MAP2, PSD95, and synaptophysin to improve synaptic plasticity. Most importantly, compared with HuA, HuA-LIP showed a superior performance against neuronal damage induced by CIH.

Conclusion: HuA-LIP has a good sustained-release effect and targeting ability and efficiently protects against neural injury caused by CIH.

Keywords: huperzine A, nanoliposomes, neuronal damage, chronic intermittent hypoxia, Iron

Introduction

Obstructive sleep apnoea (OSA) is an increasingly common sleep-breathing disorder accompanied by upper airway obstruction and arousal during sleep.[1] OSA is associated with malfunctions in multiple physiological functions, including cognition.[2] The adverse outcomes of cognitive domains manifest as daytime sleepiness, lower attention, poor episodic memory, reduced responsiveness and working memory, behavioral problems, etc.[3,4] Currently, the OSA population is increasing, and this disorder is becoming a global health problem.[5] However, most individuals remain unaware of the health problem, and 80% do not receive a diagnosis and treatment.[6]

A clinical study found that OSA patients with neurocognitive deficits had structural abnormalities in the hippocampus, parahippocampal region and prefrontal cortex.[7] Chronic intermittent hypoxia (CIH) is the primary pathological feature of OSA, and repeated hypoxic/reoxygenated cycles lead to a decrease in synaptic plasticity and memory and damage to the neurons of the hippocampus.[8,9] CIH exposure may increase the deposition of β-amyloid plaques[10] and phosphorylation of Tau protein,[11,12] accelerating the pathogenesis of Alzheimer's disease (AD). Synaptic plasticity refers

Received: 22 October 2022
Accepted: 7 February 2023
Published: 17 February 2023

to the adjustable connection strength in synapse structure and function between neurons, including long-term potentiation (LTP) and long-term depression (LTD) types.[13] LTP, which plays a critical role in memory and learning, was suppressed when subjected to CIH exposure in a duration-dependent manner. Research has also shown that CIH exposure for just seven days could decrease the synaptic plasticity manifested by cell excitability and synaptic transmission in the hippocampus of rats.[14] There are few therapeutic options for CIH-induced neural deficits at present.

It has been demonstrated in rodents that the reactive oxygen species (ROS) induced by CIH also play a vital role in neural injury.[15,16] Iron is an essential trace element; however, excess iron could accelerate ROS generation via the Fenton reaction.[17] Our previous research found that iron overload was involved in the neural damage induced by CIH.[4,16] Transferrin-transferrin receptor 1 (Tf-TfR1) is the main form of iron uptake, and inhibition of TfR1 expression attenuates the iron content in the hippocampus of CIH mice.[16] At the same time, hepcidin is the central iron regulatory factor and regulates iron exporters by causing ubiquitination and degradation of Ferroportin1 (FPN1), the sole iron exporter protein.[18,19] In the central nervous system (CNS), hepcidin is preferentially expressed in astrocytes.[18] Studies have revealed that elevated hepcidin levels contribute to neuronal iron overload in the cerebral ischemic brain[17] and neurodegenerative diseases.[19] Therefore, iron chelators and analogs used to regulate iron homeostasis have been used as a therapy for iron overload-related brain diseases.[20]

Huperzine A (HuA), isolated from the Chinese herb Huperzia Serrata, has been approved as a therapy for cognitive impairment diseases, including AD and vascular dementia.[21] HuA has been reported to reduce iron levels *in vivo and in vitro* in AD.[22,23] Our previous research showed that HuA could attenuate iron overload and synaptic dysfunction in CIH mice.[16] HuA could play a neuroprotective role; however, the blood-brain barrier (BBB) limits the final concentration in the cerebrospinal fluid.

One of the solving methods is the use of nanocarrier systems. Nanocarriers mainly include polymeric nanoparticles, nanomicelles, nanoemulsions, and liposomes. Currently, liposome is the most widely used in clinical.[24,25] Liposomal doxorubicin is the first nanodrug approved by FDA in 1995.[24] Liposomes composition is similar to biofilm, and it has excellent biocompatibility and metabolic properties.[24] The use of liposomal constructions for BBB crossing has been investigated for decades. Basic fibroblast growth factor (bFGF) packaged with nanoliposomes significantly improved bFGF accumulation in brain tissues and functional recovery induced by cerebral ischemia-reperfusion (I/R).[26] Similarly, our previous research found that nanoliposomes encapsulating lycopene[27] or ferric ammonium citrate[28] could increase the drug content in the brain. Moreover, liposomes are modified surfaces for active targeting. Such as, polyethylene glycol (PEG) increases oxaliplatin-nanoparticles prolonged circulation time, and promotes accumulation at the gastric tumor area.[25] The p-aminophenyl-α-D-manno-pyranoside (MAN) and agglutinin modified liposome could markedly improve the transport of epirubicin and resveratrol across the BBB and the survival of brain tumor-bearing animals.[29] Phosphatidylethanolamines and dioleoylphosphatidylethanolamine based nanoliposomes are more sensitive to the acid environment of cerebral ischemic penumbra.[30] In addition, a nanocarrier of oxygenation with nanobubbles is similar to the structure of liposome and could overcome hypoxic conditions in cells and enhance the delivery and release of drug, reducing complications and mortality, especially coronavirus disease.[31]

In this study, we prepared and characterized nanoliposome-encapsulated HuA based on a CIH mouse model to simulate OSA. We attempted to clarify the protective effect of HuA-LIP in synaptic plasticity and neurocognitive dysfunctions.

Materials and Methods

Reagent

Huperzine A (102518–79-6, Desite Biotechnology), soybean phosphatidylcholine (PC, L812366, Macklin), cholesterol (Chol, C804519, Macklin), potassium ferrocyanide (P3289, Sigma–Aldrich), Dihydroethidium (DHE, 19709, Cayman Chemical), toluidine blue (G1032, Servicebio), ultrapure nitric acid (6901–05, J.T. Baker), Golgi staining solution (Servicebio, G1069), the Total Superoxide Dismutase (T-SOD) assay kit (A001-1-2), Glutathione Peroxidase (GSH-Px) assay kit (A005-1-2) and Malondialdehyde (MDA) assay kit (A003-1-2) were purchased from Nanjing Jiancheng Bioengineering Institute. The RNAsimple total RNA kit (DP419, TianGen), PrimeScript^{TM} RT regent Kit with gDNA Eraser (RR047A) and SYBR-Green Premix Ex Taq^{TM} II kit (RR820A) were purchased from TaKaRa.

The antibodies used were as follows: NeuN (ab104224, Abcam), microtubule-associated protein 2 (MAP2, GB11128-2, Servicebio), transferrin receptor 1 (TfR1, 13–6800, Invitrogen), L-ferritin (FTL, ab109373, Abcam), hepcidin (DF6492, Affinity), glial fibrillary acidic protein (GFAP, GB12090, Servicebio), postsynaptic density protein 95 (PSD95, GB11277, Servicebio), growth associated protein 43 (GAP43, GB11095, Servicebio), proteinkinase A α (PKAα, sc-28315, Santa Cruz Biotechnology), synaptophysin (SYP, 17785-1-AP, Proteintech), phospho-p44/42 MAPK (p-Erk, #4376, Cell Signaling Technology), p44/42 MAPK (Erk, #9102, Cell Signaling Technology), phospho-cAMP response element binding protein (p-CREB, #9198, Cell Signaling Technology), brain derived neurotrophic factor (BDNF, GB11559, Servicebio), glyceraldehyde-3-phosphate dehydrogenase (GAPDH, GB12002, Servicebio), and β-tubulin (GB12139, Servicebio).

Preparation of Huperzine A-Liposomes

Preparation and Characteristics of HuA-LIP

Huperzine A-Liposomes (HuA-LIP) were prepared by the rotary evaporation film ultrasonication method.[32] PC, Chol and HuA were weighed at mass ratios (m_{PC}:m_{Chol} = 10:1, m_{PC}:m_{HuA} = 80:1) and dissolved in anhydrous ethanol. To prevent solvent volatilization, the beaker containing anhydrous ethanol was covered by a layer of aluminum foil during the dissolution process. Then, the solution was transferred into a round-bottom flask and evaporated at 60 rpm/min and 45 °C on a rotary evaporator. The mixture was rotated sequentially until the lipid film was hydrated and formed a suspension. Next, an appropriate amount of phosphate-buffered saline (PBS) buffer (pH = 7.4) and 2–3 mm glass beads were added to the abovementioned round-bottomed flask. The mixture was rotated for 40 min until the lipid film was hydrated and formed. The suspension was dispersed by ultrasonication for 10 min (100 W) and then dialyzed (molecular weight cut off, MWCO, 3500). The dialysate was changed every 6 h until the amount of HuA was not detectable in the dialysate. HuA-LIP was obtained and stored at 4 °C.

The encapsulation efficiency of HuA-LIP was determined using a dynamic dialysis method for dialysis and purification, and the absorbance (A308 nm) of HuA in the dialysate was tested by a UV–Vis spectrophotometer (U-3010, HITACHI, Tokyo, Japan). The HuA-LIP encapsulation efficiency (EE%) was then calculated according to the formula:

$$EE(\%) = (m - m_r)/m \times 100\%$$

where m is the total amount of HuA added initially, and m_r is the amount of unencapsulated HuA in the dialysate.

The microstructures of empty liposomes (E-LIP) and HuA-LIP were observed by transmission electron microscopy (TEM), as previously described.[27] The diameter and zeta potentials of the LIP and HuA-LIP were measured by a Zeta Sizer Nano series Nano-ZS (Malvern Instruments Ltd, Malvern, UK). Stabilization was defined as the absolute value of zeta potentials above 30 mV.

The Release of HuA-LIP in vitro

The in vitro release of HuA-LIP in PBS (pH =7.4) was studied using the dialysis diffusion technique. Briefly, 2 mL of HuA-LIP was transferred to a dialysis bag (MWCO 3500), immersed in 80 mL of release medium, incubated at 37 °C, and shaken at 60 rpm in the dark. At scheduled time intervals, 1 mL of solution was taken from the dialysate and replaced with a fresh medium to maintain a constant volume. The release amount of HuA was determined at 308 nm using ultraviolet spectrophotometry (U-3010, HITACHI, Tokyo, Japan), from which the cumulative drug release versus that of HuA-LIP was calculated using the following formula:

Cumulative drug release versus $(Q\%) = M_t/M_T \times 100\%$

where M_t is the total amount of HuA released at a certain time, and M_T is the total amount of HuA encapsulated by liposomes.

Four classical kinetic models were selected to study the in vitro release of HuA-Liposome:

Zero-order kinetic model: $Q = k_0 t + A$ (1)

First-order kinetic model: $Q = A(1 - \exp(-k_1 t))$ (2)

Higuchi model: $Q = k_H t^{0.5} + A$ (3)

Weibull model: $Q = A(1 - \exp(-(k_w(t - tb))^c)$ (4)

In the formulas, Q refers to the amount of drug release, and k is the release rate constant.

Animals and Groups

Male C57BL/6N mice (22–24 g) were purchased from Beijing Vital River Laboratory Animal Technology Co., Ltd. (Beijing, China). All mice were housed at the Animal Centre and acclimatized to their environment for one week. Animal experiments strictly complied with the National Institutes of Health Guide for the Care and Use of Laboratory Animals and were approved by the Animal Care and Use Committee of Medical Ethics of Hebei University of Chinese Medicine (NO. DWLL2018007).

The experimental animals were divided into four groups: normal control (Con) group, CIH group, HuA-LIP group, and HuA group (n = 10 each group). The CIH model was set up to mimic the chronic hypoxia and reoxygenation of OSA patients. Mice were exposed to a hypoxic chamber with an oxygen concentration from 21% to 5% in the first 1.5 min and then returned to 21% in another 1.5 min (Figure 1B). Mice were exposed to CIH for 21 days, 8 h per day. The mice

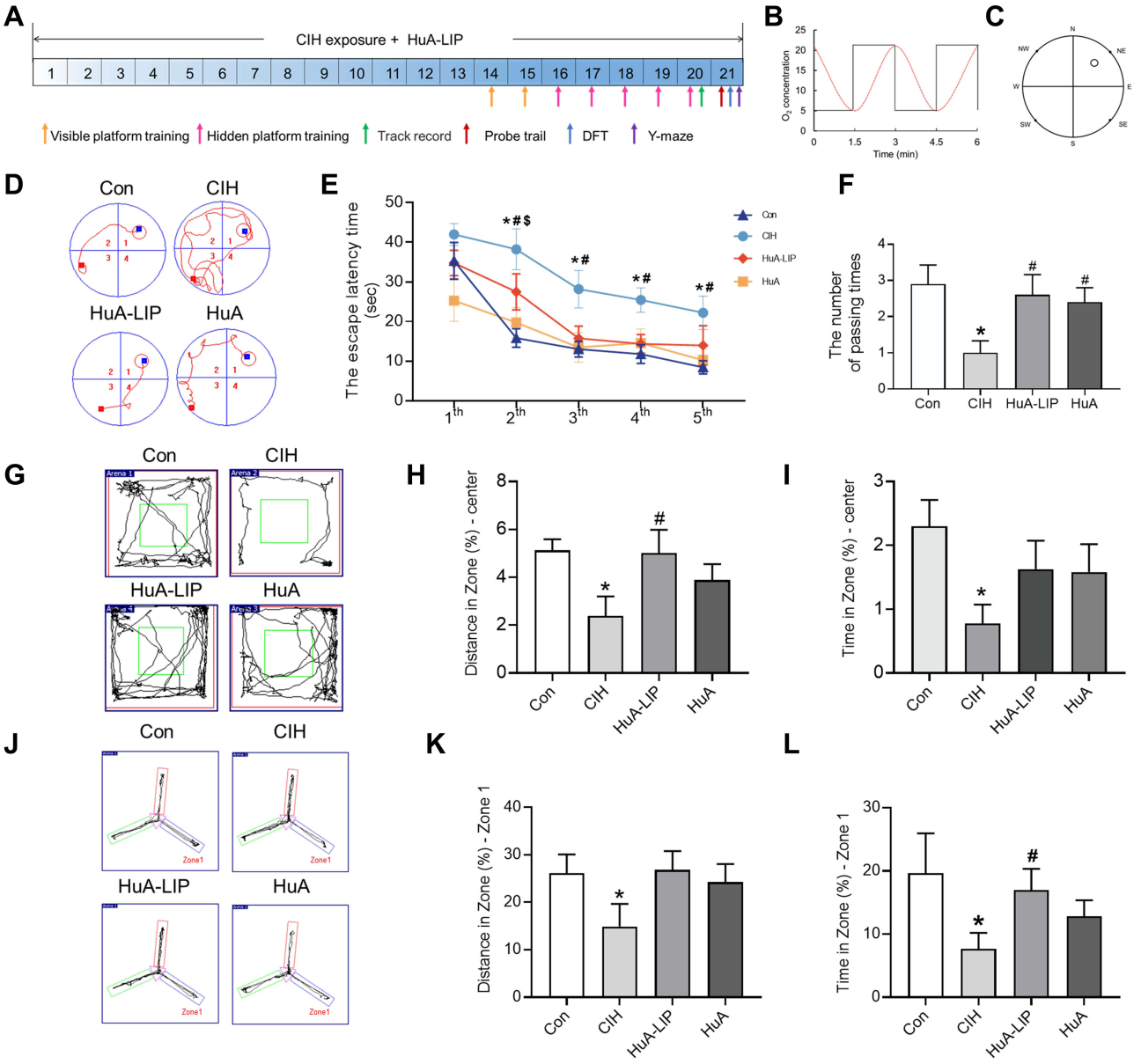

Figure 1 Ethological measurement of mice exposed to 21 days of CIH. (**A**) The flow chart of ethological measurement, CIH exposure and HuA-LIP administration. (**B**) The flow chart of experimental CIH exposure. (**C**) The images of water maze platform. (**D**) The escape track record. (**E**) The escape latency time. (**F**) The number of passing times of probe trial. (**G**) The trajectories of squares in OFT test. (**H**) The distance spent in the centre zone. (**I**) The time spent in the centre zone. (**J**) The trajectories in the Y-maze. (**K**) The distance spent in the centre zone 1. (**L**) The time spent in the centre zone 1. The results are presented as the mean ± SEM (n = 10). Normal control group (Con), Chronic intermittent hypoxia group (CIH), Huperzine A-Liposomes group (HuA-LIP), Huperzine A group (HuA). *p < 0.05 vs Con group. $^{\#}p$ < 0.05 vs CIH group. $^{\$}p$ < 0.05 vs HuA-LIP group.

inhaled normal air and were exposed to identical chambers in the Con group. The CIH mice were administered HuA (0.1 mg/kg/day, i.p.) for 21 days in the HuA group.[33] The CIH mice in the HuA-LIP group received HuA-LIP, which consisted of equal contents of HuA. The mice in the CIH group received an equal volume of empty liposomes.

Behavioral Tests

Morris water maze (MWM) was used to evaluate spatial memory, as previously described.[4] As shown in Figure 1A, two days of visible platform training were used to adapt the mice to the aquatic labyrinth. Then, the following five days of hidden platform training were used to place the navigation test. The pool (diameter = 100 cm) was divided into 4 equal quadrants (N, S, E, W) (Figure 1C). Each mouse was placed into the pool from four different starting positions (NE, SE, SW, NW). The escape distance traveled to reach the escape platform and the time spent reaching the platform were recorded. The escape distance and time from SW to the platform were recorded and quantified by the Smart Video Tracking System (Smart version 2.5, Panlab, Barcelona, Spain). The hidden platform was removed for the probe trial on the 6th day. The number of times the platform passed was recorded within 2 min.

The open-field test (OFT) was performed on the 21st day after CIH exposure (Figure 1A) to elevate the ability of spontaneous movement. The open field facility is a black plastic open field box with dimensions of 40×40×45 cm^3. The centers (20×20 cm^2) were divided by red lines at the bottom of the open field box. Mice were placed into the centers on the bottom of the box. Each open file box was rubbed with alcohol to prevent interference from animal residues at the end of each test. The total movement distances were recorded within 5 min by the camera located above the open field box. The time and movement distance of staying in the center area were analyzed by SMART software.

The Y maze test was also performed on the 21st day after CIH exposure to elevate working memory (Figure 1A). The apparatus for the Y maze was made of black plastic; each arm was 40 cm long, 12 cm high, 3 cm wide at the bottom, and 10 cm wide at the top. The three arms were connected at an angle of 120°. Each arm had a movable partition in the center; three arms of each Y-maze were randomly assigned as New Arm (Zone 1), Starting Arm (Zone 2), and Other Arm (Zone 3). New arm: in the first stage of the experiment (ie, the training period), the baffle was blocked; in the second stage (ie, the test period), it was opened. Starting arm: the arm through which the mouse enters the maze. The starting arm and the other arm were kept open throughout the experiment, allowing the animals to come and go freely. The maze was covered with wood shavings. At the end of each training or test, each arm was rubbed with alcohol to prevent interference from animal residues. A camera lens was placed 1.5 m above the maze to record the entire process.

Pathological Staining

Hematoxylin and eosin (H&E) staining was applied to observe the basic structure of hippocampal tissue. The hippocampal paraffin sections (5 μm) were dewaxed with xylene and rehydrated with gradient alcohols. Then, the sections were stained with hematoxylin, differentiated with hydrochloric acid ethanol, and redyed with eosin. Finally, the sections were dehydrated with gradient alcohol, and vitrified with xylene.

Nissl staining was performed as previously described.[16] After deparaffinization, the sections were stained with 1% toluidine blue for 30 min at room temperature. Then, the sections were dehydrated, vitrified and sealed. The whole and enlarged hippocampus were visualized by electron microscopy (DM3000, Leica, Solms, Germany). The mean density of Nissl bodies was calculated by IPP Image-Pro Plus 6.0 software (IPP 6.0, Media Cybernetics, USA).

Immunohistochemistry

The paraffin sections were dewaxed and rehydrated, incubated with 3% H_2O_2 and antigen repaired with citrate buffer. The sections were blocked with 10% goat serum at 37 °C and drained. The sections were incubated with primary antibodies against NeuN, MAP2, and p-CREB overnight at 4 °C. On the second day, the sections were incubated with the HRP-conjugated secondary antibody and then the DAB staining solution. The mean density of immune-positive proteins was measured and calculated by IPP 6.0 software.

At the same time, the sections were incubated with a mixture of rabbit anti-hepcidin or anti-FTL and mouse anti-GFAP or anti-NeuN bodies at 4 °C overnight. Then, the secondary antibodies, a mixture of 549 goat anti-rabbit IgG and 488 goat anti-mouse IgG, were added to the sections and incubated for 1 h at 37 °C. Finally, the sections were sealed with

an anti-fluorescence quencher (containing DAPI dye) and imaged under a fluorescence microscope (THUNDER DMI8, Leica, Solms, Germany).

Iron Content Measurement

Perls' Staining

Perls' reagent, also called Prussian blue, was applied to detect ferric iron in the hippocampus. The sections were dewaxed, and incubated in 3% H_2O_2 for 20 min at room temperature (RT). Then, the sections were immersed in fresh Perls' reagent (containing 1% potassium ferrocyanide and hydrochloric acid) for 12 h at RT. After washing with PBS, the sections were stained with DAB for 10 min at RT. Finally, the sections were dehydrated, hyalinized and sealed. The mean Fe density was calculated by IPP 6.0 software.

ICP-MS

The total iron content in hippocampal tissue was determined by inductively coupled plasma–mass spectrometry (ICP–MS, Thermo Fisher Scientific, Waltham, MA, USA).[19] Before the experiments, the hippocampal tissues were dried and weighed. The dried tissues were put into Teflon digestion tubes and digested with 1 mL of ultrapure nitric acid (69.9–70.0%; J.T. Baker, Phillipsburg, NJ, USA). When the tissues were completely digested, 2 mL of ultrapure water was added for resolution. Iron standard curves were prepared ranged from 0 to 100 ppb in 0.2% nitric acid. ICP–MS measured the blanks and digested samples, and then the total iron content was calculated.

Oxidative Stress

DHE staining was used to detect superoxide free radicals in the hippocampus. The sections were incubated with an autofluorescence quencher and then added to 5 μM DHE at 37 °C for 30 min. Finally, the sections were sealed with an anti-fluorescence quencher (containing DAPI dye) and imaged under a fluorescence microscope (THUNDER DMI8, Leica, Solms, Germany).

The hippocampal tissues were prepared into 10% (g/V) homogenate, and the protein concentration was measured using the BCA method. The T-SOD activity, GSH-Px enzyme activity, and MDA content were measured separately according to each manufacturer's instructions. Finally, the absorbance levels of SOD (550 nm), GSH-Px (412 nm), and MDA (550 nm) were detected and calculated.

Golgi Staining

The hippocampal tissues were immersed in Golgi staining solution and stored in the dark for 14 days, according to the manufacturer's instructions. After washing with distilled water, they were immersed in 80% glacial acetic acid for 12 h and then placed into 30% sucrose. The tissues were cut into 100 μm sections, pasted onto a gelatine slide, and dried in the dark overnight. After developing and fixing, the sections were imaged by a microscope.

Transmission Electron Microscopy (TEM)

After deep anaesthetization, the hippocampal tissue (1 cm^3) was promptly removed and fixed in electron microscopy fixation fluid. Then, the samples were prepared according to standard procedures as previously described.[4] The sections were observed under a Hitachi HT7800/HT7700 electron microscope.

Western Blot

Protein extraction and sample preparation were performed as previously described.[16] The blots were incubated with primary antibodies against TfR1, PSD95, SYP, GAP43, PKAα, p-ErK, ErK, BDNF, β-tubulin or GAPDH at 4 °C overnight. On the following day, the blots were washed and incubated with secondary antibodies for 60 min at RT. The immunoreactive protein bands were imaged by the enhanced chemiluminescence method, and the mean grey value was calculated by ImageJ software (Rawak Software Inc., Stuttgart, Germany).

Table 1 The Sequence of Primers Used for the Expression of Genes

Gene	Forward Primer	Reverse Primer	Length
Hepcidin	AGACATTGCGATACCAATGCA	GCAACAGATACCACACTGGGAA	108 bp
β-actin	AGGCCCAGAGCAAGAGAGGTA	TCTCCATGTCGTCCCAGTTG	81 bp

RT-PCR

Total RNA in the hippocampus was extracted via an RNA extraction kit, and then 1 μg of RNA was reverse-transcribed into cDNA. PCR amplification was quantitated by a SYBR-Green PCR Master Mix kit in a real-time quantitative PCR instrument (CFX Connect, Bio-Rad Laboratories, Hercules, CA, USA). The primer sequences are shown in Table 1. The hepcidin relative gene expression was calculated by the $2^{-\Delta\Delta Ct}$ formula.

Iron Ions Interaction

Analysis of interaction with iron ions was carried out as previously described.[34] HuA, dissolved in methanol, reacted with Fe^{2+} and Fe^{3+} solutions in acetic acid-sodium acetate (HAc-NAc) buffer. Then HuA and mixture were simultaneously detected via full wavelength scanning. The λ absorption was recorded at 200–900 nm.

Statistical Analysis

The obtained results are presented as the mean ± SEM. The data were analyzed by SPSS 23.0 (SPSS Inc., Chicago, IL) software using one-way ANOVA followed by the LSD post hoc test or *t*-test. Two-way ANOVA was used to analyze the data from the MWM. A $p < 0.05$ was regarded as the significance level. The statistical charts were created by GraphPad Prism 9.0 software (GraphPad Software, Inc., La Jolla, CA).

Results

The Characteristics and Stability of HuA-LIP

As shown in Figure 2A and B, HuA was packaged with liposomes in HuA-LIP. Because HuA was hydrophobic, and it would enter into the bilayer of the liposome. TEM results indicated that the empty liposomes (E-LIP) and HuA-LIP were spherical vesicles, and both diameters were less than 100 nm (Figure 2C and D). The size of HuA-loaded liposomes was less than that of the empty liposomes due to the hydrophobic-hydrophobic interaction between HuA and the liposomes' bilayer. The diameters of E-LIP and HuA-LIP were mainly distributed in the range of 32.67–105.7 nm and 13.54–43.48 nm, respectively (Figure 2E and F), corresponding to the figure shown in Figure 2C and D. The means of the zeta potentials were −45.5 mV (E-LIP) and -47.1 mV (HuA-LIP), which indicated that the liposomes were stable (Figure 2G and H). Zeta potential technology was applied to investigate the structural stability of HuA-LIP in aqueous dispersion. When the absolute value of the zeta potential is greater than 30 mV, the charge of liposomes inhibits coalescence and possesses good stability.[35]

The in vitro release of HuA-LIP could predict the drug efficacy in vivo and contributes to establishing the in vitro–in vivo correlation. The common dynamics models included zero-order kinetics (Figure 3A), first-order kinetics (Figure 3B), Higuchi (Figure 3C) and Weibull models (Figure 3D). The in vitro release data of HuA-LIP fitted with different models are shown in Table 2. The release of HuA-LIP belonged to a first-order kinetic model according to the maximum value of R^2 ($R^2 = 0.9740$). It indicated that HuA had a constant elimination half-life, which was independent of the concentration of HuA. It suggested that HuA-LIP could release continuously for a long time; that was, HuA-LIP had a long-sustained release property. In summary, we established a protocol for encapsulating HuA with liposomes, accompanied by stable physicochemical properties and long-term stability.

HuA-LIP Observably Improved Cognitive Dysfunction Induced by CIH Exposure

The cognitive deficit has been reported in rodents exposed to CIH.[8] Similarly, we found that CIH mice showed a more complicated escape route (Figure 1D), longer escape time (Figure 1E), and fewer passing times (Figure 1F). HuA and

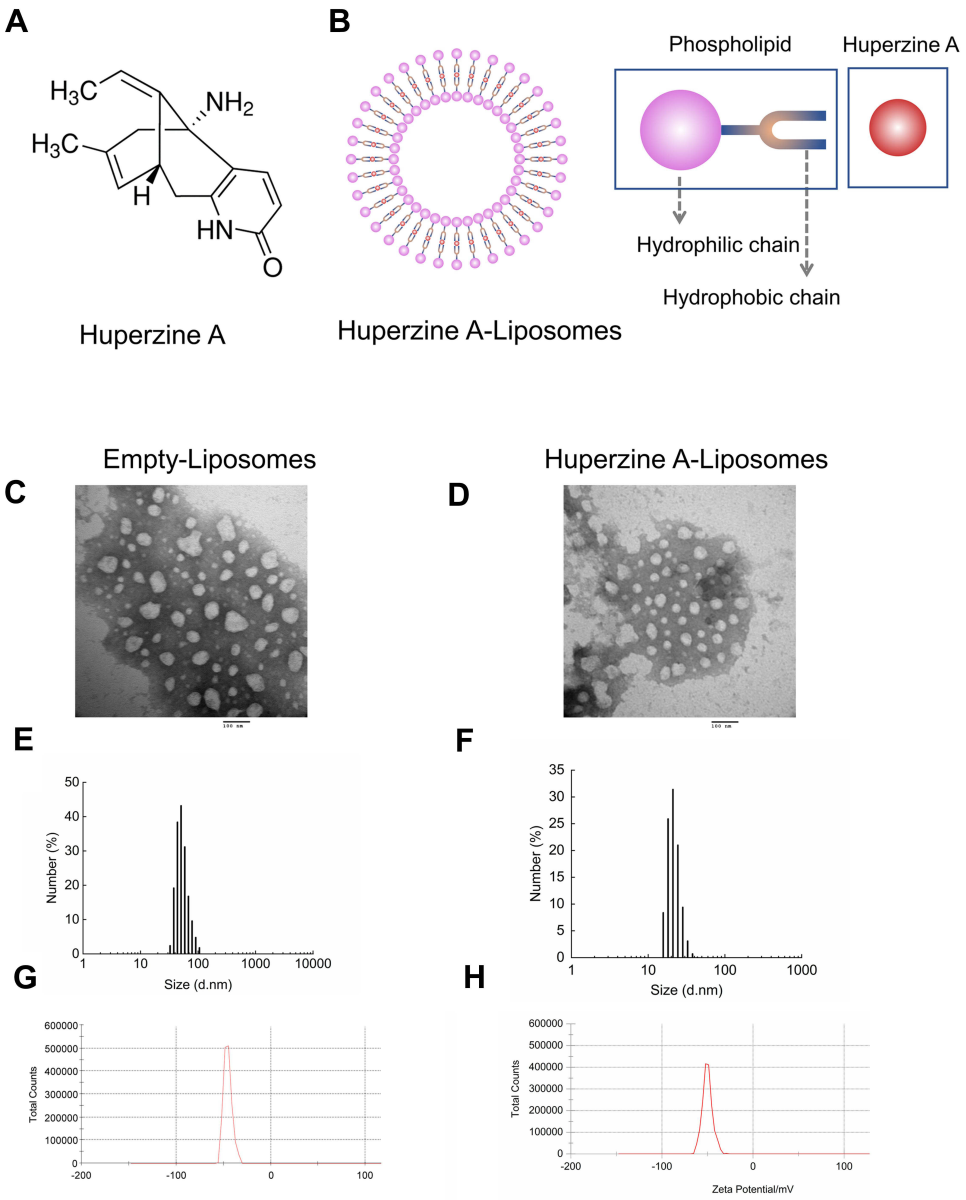

Figure 2 Characterization of Huperzine A-Liposomes. (**A**) The chemical structure of Huperzine A. (**B**) The structural model of Huperzine A-Liposome. (**C** and **D**) The TEM images of Empty-Liposome and Huperzine A-Liposome (Scale bars = 100 nm). (**E** and **F**) The diameter of Empty-Liposome and Huperzine A-Liposome by DLS. (**G** and **H**) The Zeta-potential of Empty-Liposome and Huperzine A-Liposome.

HuA-LIP administration relieved the cognitive dysfunction induced by CIH (Figure 1D–F). However, the neuroprotection of HuA-LIP showed a better effect.

OFT was used to elevate locomotory and exploratory activity. CIH exposure impeded the exploring activity of mice, as manifested by decreased distance and time of entries into the center zone (Figure 1G–I). Dysfunction was improved when treated with HuA-LIP; however, the improvement in HuA was not significant. The Y-maze was applied to evaluate short-term memory. As shown in Figure 1J–L, Y-maze alternations were reduced when exposed to CIH; however, the difference was insignificant in treated groups. Taken together, these ethological results demonstrated that CIH significantly decreased long-term memory, and HuA-LIP presented improvement in cognitive dysfunction.

HuA-LIP Significantly Attenuated Neuronal Damage in the Hippocampus of CIH Mice

Memory disorder is related to neuronal injury in the hippocampus. As shown in Figure 4A, CIH mice showed cell body shrinkage, cytoplasm concentration, and nuclear pyknosis in neuronal cells. The density of Nissl bodies (Figure 4B and C)

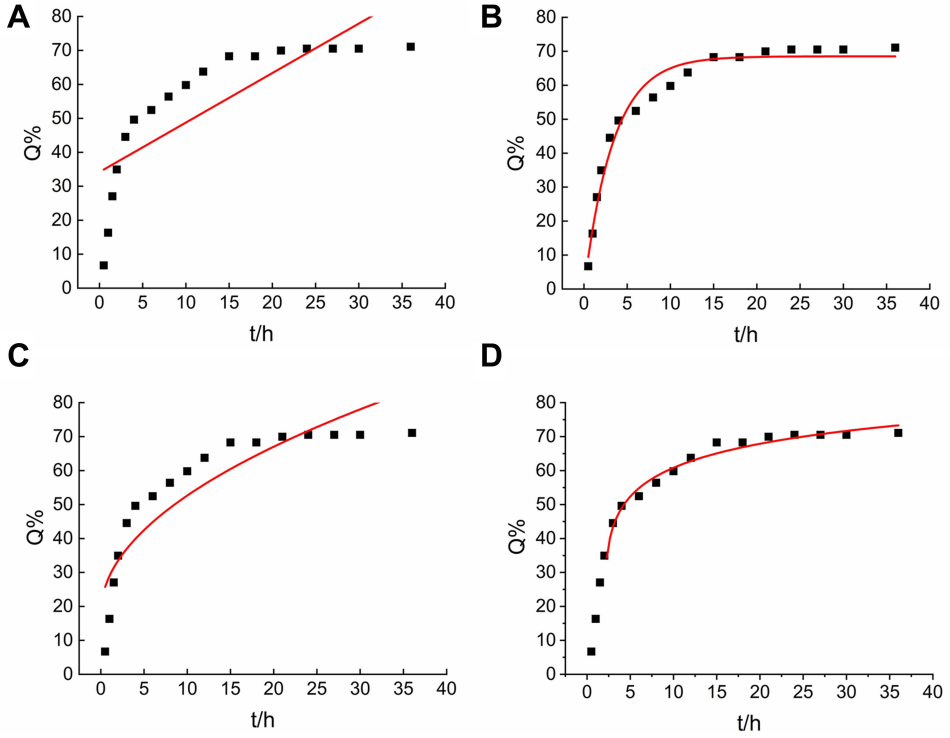

Figure 3 The release of Huperzine A-Liposomes in vitro. (**A**) Zero-order kinetics. (**B**) First-order kinetics. (**C**) Higuchi models. (**D**) Weibull models.

and neurons (Figure 4D and E) was lower in the hippocampus of CIH mice and higher after HuA and HuA-LIP administration. Meanwhile, the neuroprotection of HuA-LIP was superior to that of HuA ($p < 0\ 05$). These results indicated that HuA-LIP could improve the neuronal damage induced by CIH.

HuA-LIP Markedly Decreased Excessive Iron in CIH Mice

Excessive iron has been reported to be involved in memory deficiency in CIH mice.[4] The ferric iron (Figure 5A and B) and total iron (Figure 5C) were all increased in the hippocampal tissue induced by CIH. The elevated iron levels all declined with HuA and HuA-LIP administration, and more change was shown in the HuA-LIP group than in the HuA group (Figure 5A–C). The chelating experiment showed λ absorption spectra did not change when reacting with Fe^{2+} and Fe^{3+} (Figure 5D). Simultaneously, we detected the expression of iron-related proteins in neurons. The hepcidin mRNA was higher during CIH (Figure 5E). The hepcidin protein in the astrocyte (marked by GFAP) was elevated, as shown by immunofluorescence (Figure 5F). The expression of TfR1 protein increased when exposed to CIH (Figure 5G). The total FTL protein level was upregulated in the hippocampus tissue (Figure 5H), and immunofluorescence revealed a higher level of FTL in neurons (Figure 5I). These data indirectly indicated that iron was overloaded in the neurons after CIH treatment, which were restrained by HuA-LIP treatment. Compared to the HuA group, HuA-LIP better downregulated the expression of TfR1. Overall, the data demonstrated that HuA-LIP more efficiently reduced iron levels in CIH mice.

Table 2 The Fitting Results of HuA-LIP Release

	Models	Fitting Results	R^2
HuA-LIP	Zero-order kinetics	Q% = 34.21 + 1.457t	0.6199
	First-order kinetics	Q% = 68.51(1 - exp(−0.2973t))	0.9740
	Higuchi	Q% =10.96t^0.5 + 17.99	0.8047
	Weibull	Q%=1+37.89exp(0.0225t)-1.62E8exp(2.14E7t)	0.5461

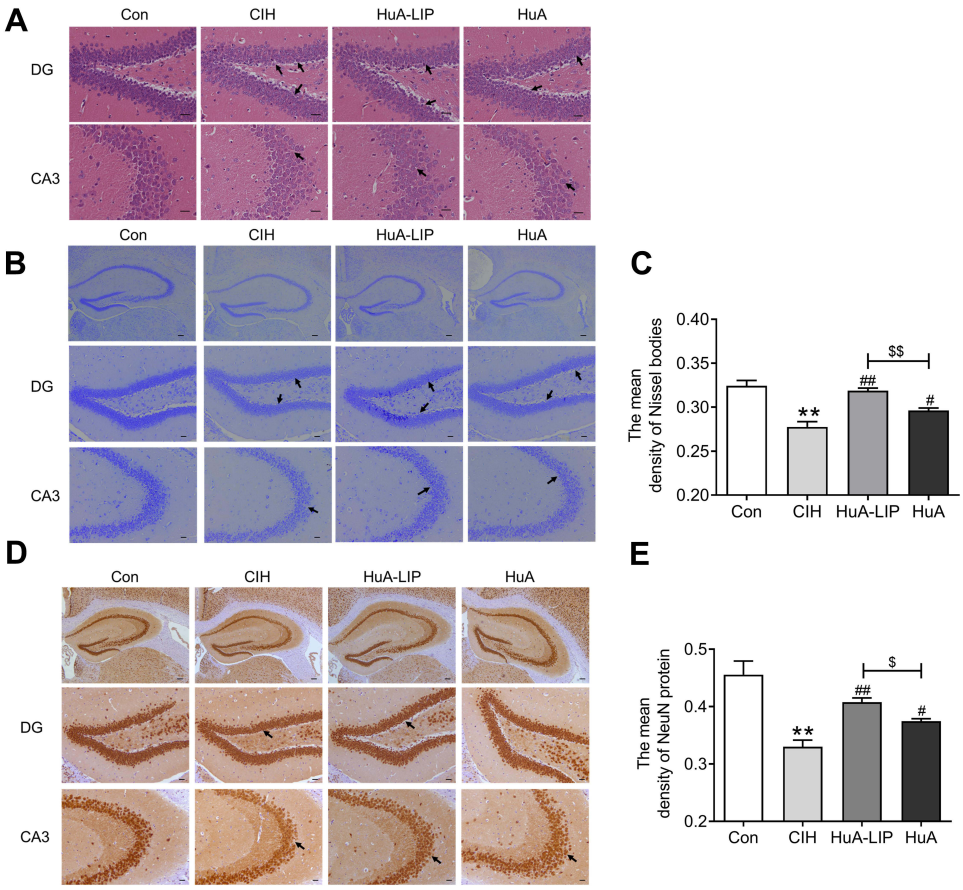

Figure 4 Damage of neurons in the hippocampus of CIH mouse. (**A**) H&E staining of hippocampus with Con, CIH, HuA-LIP, HuA groups (Scale bar = 25 μm, n = 3). (**B**) The Nissl's staining (Scale bar = 25 μm). (**C**) The mean density of Nissl bodies as shown in panel B (n = 3). (**D**) The immunohistochemical staining of NeuN protein (Scale bar = 25 μm). (**E**) The mean density of NeuN protein as shown in panel D (n = 3). The results are presented as the mean ± SEM. Normal control group (Con), chronic intermittent hypoxia group (CIH), Huperzine A-Liposomes group (HuA-LIP), Huperzine A group (HuA). $^{**}p < 0.01$ vs Con group. $^{\#}p < 0.05$, $^{\#\#}p < 0.01$ vs CIH group. $^{\$}p < 0.05$, $^{\$\$}p < 0.01$ vs HuA-LIP group.

HuA-LIP Visibly Reduced Oxidative Stress in Hippocampal Tissue of CIH Mice

Because excessive iron could promote oxidative damage, we next assessed the ROS level and peroxidation product content. DHE staining revealed that the fluorescence signal in CIH mice was decreased after treatment with HuA and HuA-LIP (Figure 6A). Compared to HuA mice, HuA-LIP mice showed a more vital ability to protect against the increased ROS (Figure 6A). At the same time, the T-SOD and GSH-Px activities, indicators of antioxidant capacity, were decreased in the CIH mice (Figure 6B and C). MDA, one of the lipid peroxidation products, was increased in the CIH mice (Figure 6D). The lower SOD and GSH-Px levels and higher MDA levels were normalized in the HuA and HuA-LIP groups (Figure 6B–D). HuA-LIP presented a slight advantage over HuA; however, there was no significant difference. Taken together, these results demonstrated that HuA-LIP increased the antioxidant ability against CIH-induced neuronal injury.

HuA-LIP Prominently Improved Synaptic Spine Density in CIH Mice

To further assess neuronal synapse function, Golgi staining and synapse-associated proteins were measured in the hippocampus. As shown in Figure 7A, there was a small reduction in the overall spine density after 21 days of CIH, which was partially improved by HuA and HuA-LIP treatment. TEM images revealed that the thickness and length of postsynaptic density (PSD) decreased compared to the normal (Figure 7B). Compared to the Con group, the expression of PSD95 (Figure 7C) and SYP (Figure 7D) was decreased in the CIH group, while the GAP43 (Figure 7E) level showed

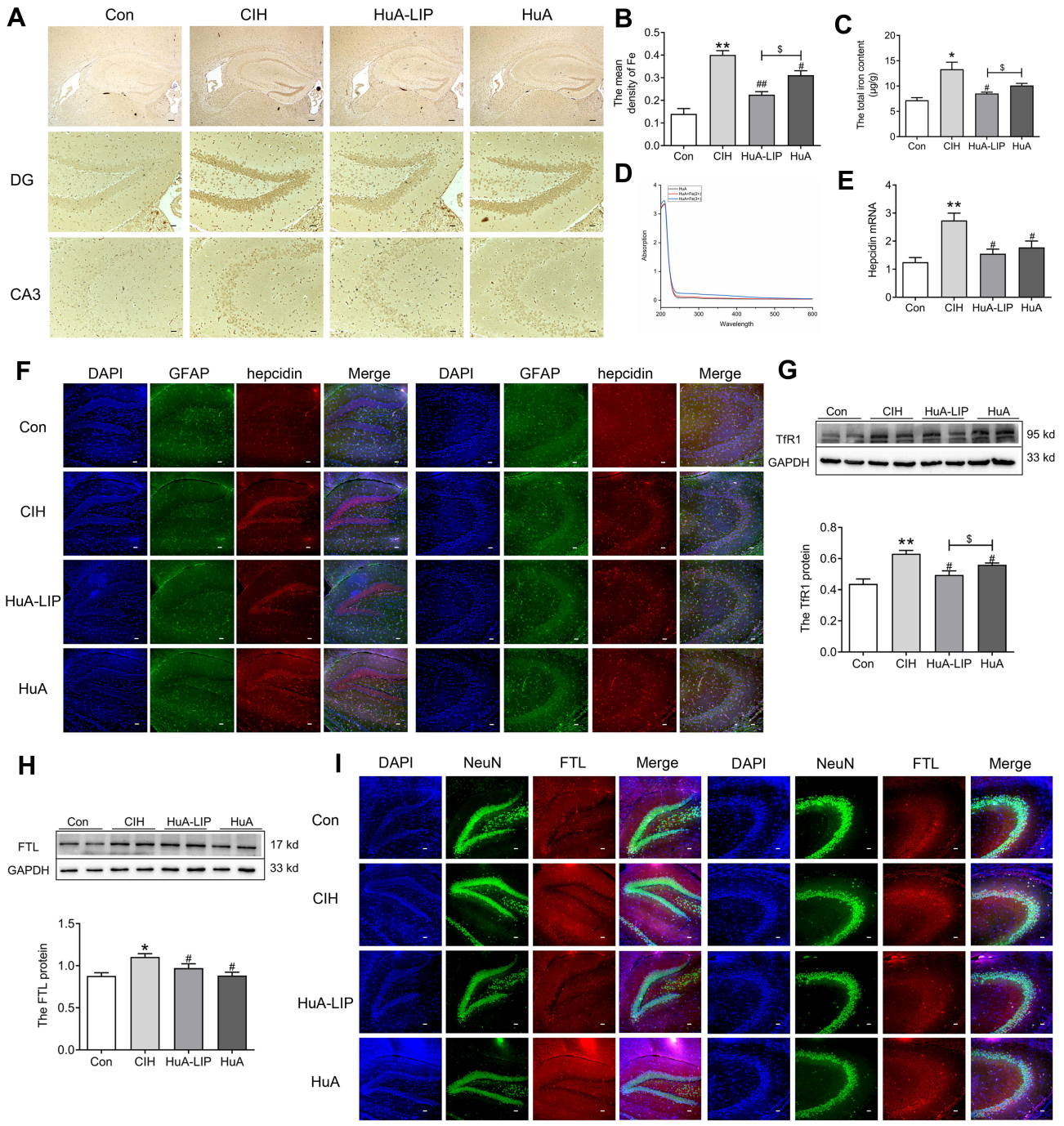

Figure 5 Iron levels in the hippocampus of CIH mice. (**A**) Perls' staining in the hippocampus (Scale bar = 25 μm). (**B**) The mean density of Fe content as shown in panel A (n = 3). (**C**) The total iron content in the hippocampus tissue measured by ICP–MS (n = 3). (**D**) The λ absorption of HuA with Fe^{2+} and Fe^{3+}, respectively. (**E**) The expression of hepcidin mRNA (n = 5). (**F**) The sections were labelled for DAPI (blue), GFAP (green), and hepcidin (red) (scale bar = 25 μm, n = 3). (**G**) The expression of TfR1 proteins measured by Western blot (n = 6). (**H**) The FTL proteins measured by Western blot (n = 6). (**I**) The sections were labelled for DAPI (blue), NeuN (green), and FTL (red) (scale bar = 25 μm, n = 3). The results are presented as the mean ± SEM. Normal control group (Con), Chronic intermittent hypoxia group (CIH), Huperzine A-Liposomes group (HuA-LIP), Huperzine A group (HuA). $^{*}p < 0.05$, $^{**}p < 0.01$ vs Con group. $^{\#}p < 0.05$, $^{\#\#}p < 0.01$ vs CIH group. $^{\$}p < 0.05$ vs HuA-LIP group.

no significant difference. Damaged synapses and lower levels of PSD95 and SYP were elevated when the animals were treated with HuA and HuA-LIP (Figure 7C and D). Furthermore, the administration of HuA-LIP exhibited a slight advantage over HuA.

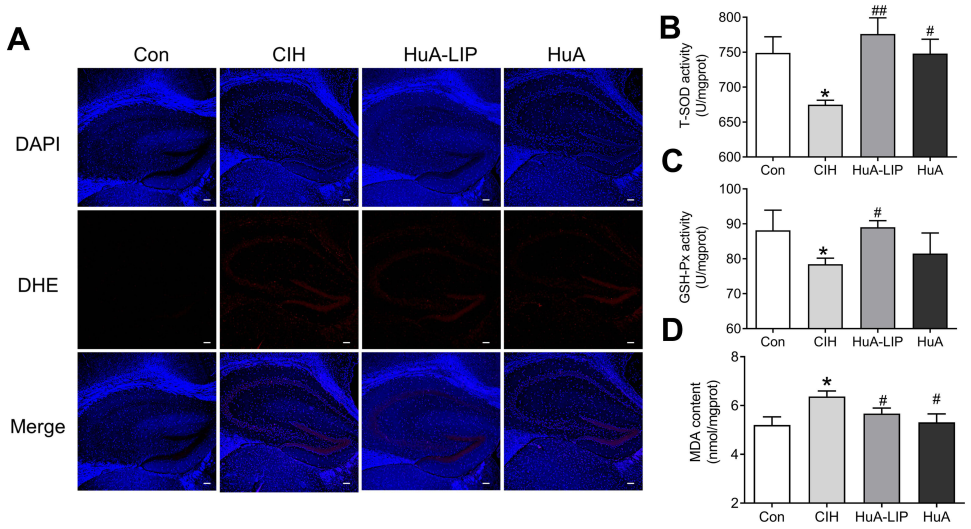

Figure 6 Oxidative stress injury in the hippocampus of CIH mice. (**A**) The DHE staining in the hippocampus (Scale bar = 25 μm, n = 3). (**B** and **C**) The T-SOD and GSH-Px activity in the hippocampus tissue (n = 5). (**D**) The MDA content in the hippocampus tissue (n = 5). The results are presented as the mean ± SEM. Normal control group (Con), chronic intermittent hypoxia group (CIH), Huperzine A-Liposomes group (HuA-LIP), Huperzine A group (HuA). $^{*}p < 0.05$ vs Con group. $^{\#}p < 0.05$, $^{\#\#}p < 0.01$ vs CIH group.

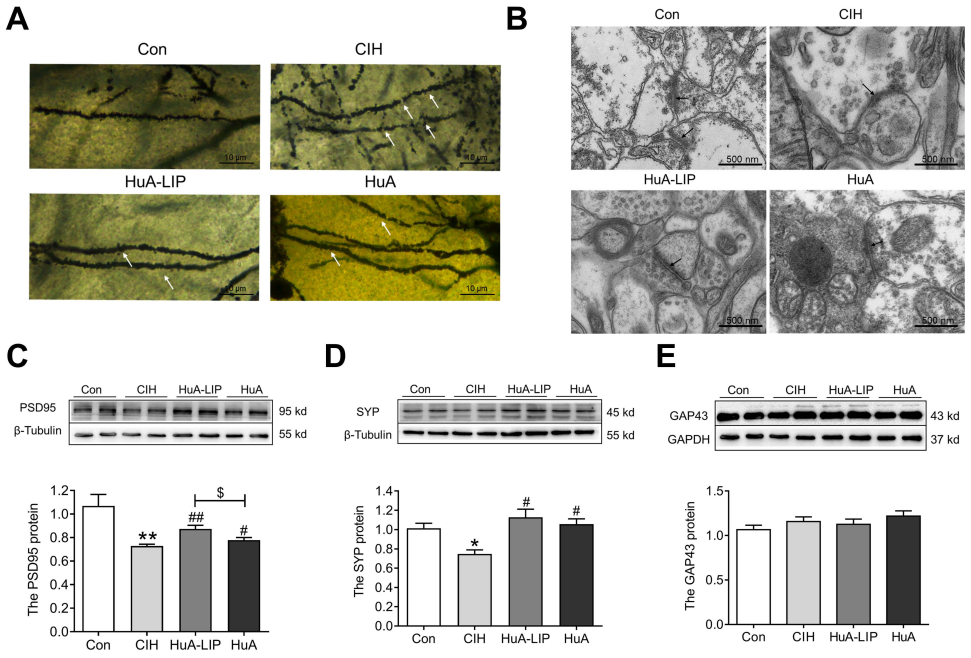

Figure 7 The impairment of synaptic function in the hippocampus of CIH mice. (**A**) The Golgi staining (n = 3). (**B**) The synaptic images of TEM in the hippocampus (n = 3). (**C**–**E**) The expression of PSD95, Synaptophysin (SYP) and GAP43 proteins by Western blot (n = 6). The results are presented as the mean ± SEM. Normal control group (Con), chronic intermittent hypoxia group (CIH), Huperzine A-Liposomes group (HuA-LIP), Huperzine A group (HuA). $^{*}p < 0.05$, $^{**}p < 0.01$ vs Con group. $^{\#}p < 0.05$, $^{\#\#}p < 0.01$ vs CIH group. $^{\$}p < 0.05$ vs HuA-LIP group.

PKAα/Erk/CREB/BDNF Signaling Pathway is Involved in the Neuroprotection of HuA-LIP

To explore the mechanism of synaptic damage, we measured the related signaling pathways. MAP2 levels were significantly decreased in CIH mice, indicating that synaptic transmission of neuronal cells was partly inhibited (Figure 8A and B). HuA and HuA-LIP treatment restored the lower level of MAP2, and HuA-LIP was more effective (Figure 8A and B). We also found that the PKAα levels, the ratio of p-Erk/Erk, and BDNF levels were downregulated in CIH mice (Figure 8C and E). Immunohistochemical staining revealed that the p-CREB levels also decreased in the

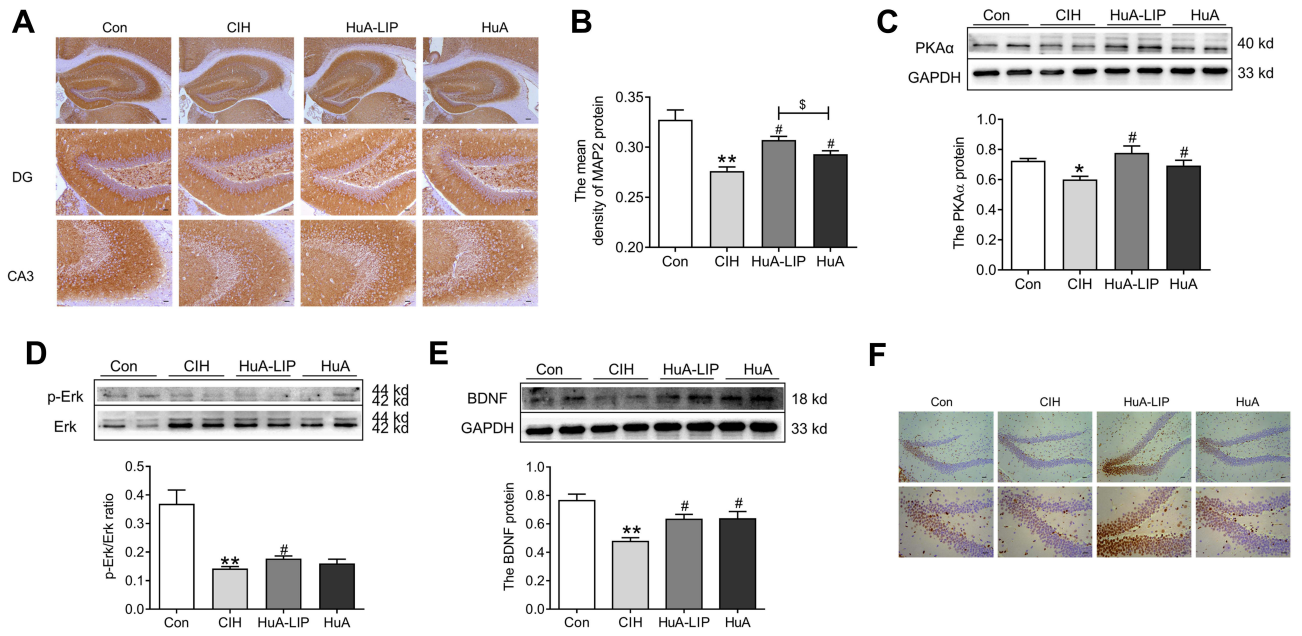

Figure 8 The PKAα/Erk/CREB/BDNF signal pathway expression in the hippocampus tissue. (**A**) The immunohistochemical staining of MAP2 protein (Scale bar = 25 μm). (**B**) The mean density of MAP2 protein as shown in panel A (n = 3). (**C**) The expression of PKAα protein (n = 6). (**D**) The ratio of p-Erk/Erk (n = 4). (**E**) The expression of BDNF proteins (n = 6). (**F**) The immunohistochemical staining of p-CREB protein (Scale bar = 25 μm, n = 3). The results are presented as the mean ± SEM. Normal control group (Con), chronic intermittent hypoxia group (CIH), Huperzine A-Liposomes group (HuA-LIP), Huperzine A group (HuA). *$p < 0.05$, **$p < 0.01$ vs Con group. $^{\#}p < 0.05$ vs CIH group. $^{\$}p < 0.05$ vs HuA-LIP group.

hippocampus of CIH mice (Figure 8F). HuA and HuA-LIP indeed relieved the inhibition of the PKAα/Erk/CREB/BDNF signaling pathway during CIH, and the effect of HuA-LIP was more significant.

Discussion

OSA is featured with CIH and sleep fragmentation, which has been proven to be associated with oxidative damage and neurocognitive disfunctions.[9] Therefore, administering antioxidant and neuroprotective agents may be beneficial. HuA has been wildly used to prevent and cure dementia-like diseases. HuA is a drug with poor water solubility and low bioavailability. Clinically, the common available pharmaceutical forms of HuA include oral dosages and injections. Owing to the rapid metabolism, HuA should be frequently administered to maintain efficient plasma concentration.[36] BBB significantly complicates drug delivery into the brain tissues.[24] Therefore, various nanocarrier systems of HuA are explored in animal models, such as microneedles,[36] self-microemulsifying,[37] and lactoferrin-loaded nanoemulsion.[38] In this study, we encapsulated HuA into nanoliposomes and tried to produce a more efficient delivery system. Liposomes carry HuA within the lipid bilayer structure, fuse with cellular membranes and release HuA into cytoplasm (Figure 2). At the same time, zeta potential technology showed HuA-LIP in aqueous dispersion owned steadily structural stability, and the nanosized liposomes could more readily cross BBB.[24] Therefore, we successfully prepared nanoscale HuA-LIP with a small diameter and high stability and comprehensively evaluated the possible mechanism of ameliorating neuronal injury.

CIH exposure has been previously demonstrated to impair synaptic plasticity and working memory. Synaptic plasticity is often manifested as changes in the PSD.[39] The shorter and smaller thickness of PSD has been observed in the hippocampus of CIH mice under an electron microscope.[4,8] PSD95 is the most abundant protein in PSD; it can bind to N-methyl-d-aspartic acid receptor (NMDARs) subtype and then anchor to the postsynaptic membrane, enhancing stability and synaptic plasticity.[40] PSD95 can also contribute to the formation of dendritic spines, which are involved in synapse formation and maturation.[41,42] SYP is the abundant transmembrane protein in synaptic vesicles (SVs), engaged in SVs cycling and endocytosis, and it is considered a specific indicator for SVs.[13] The decreased SYP protein levels suggested a decline in the number of SVs and neurotransmitters, resulting in reduced presynaptic excitability.[16] In our

study, the cognitive function after exposure to 21 days of CIH may be related to the abnormal PSD structure, lower PSD95 and SYP levels (Figure 7).

BDNF was proven to play an important role in neuroprotection and neuronal plasticity in CNS diseases by maintaining LTP.[43,44] OSA patients, those with higher level of BDNF, showed a declined neurocognitive impairment.[45] Using BDNF treatment, the LTP deficit induced by CIH will be rescued.[14] As a neurotrophin, BDNF can also directly affect the maturation of neurons.[46] Therefore, elevating BDNF levels may be an effective treatment for neurological damage induced by CIH. Hypoxia could lead to anaerobic respiration and result in the restriction in cell viability and ATP production. This leads to an increase in adenosine monophosphate (cAMP) and adenosine in the cells that is secreted into the synapse to decrease synaptic transmission through adenosine A1 auto receptors.[14] The cAMP/PKA plays a role in the consolidation phase of memory. The PKA can directly cause CREB activation through phosphorylation on Ser133.[14] Then, the phosphorylated CREB will bind to the promoter of BDNF and enhance the transcription of BDNF.[16] At the same time, PKA could activate Erk1/2 phosphorylation and then lead to CREB activation.[47] In addition, phosphorylated Erk1/2 can phosphorylate ephrin-B3 and then affect the recruitment of PSD95 at the synapse.[48] A previous study has shown that CIH reduces the availability of cyclic cAMP and then reduces the activation of CREB.[14] Li et al demonstrated that increasing cAMP levels can ameliorate endothelial barrier disruption induced by CIH.[47] Therefore, the suppression of the PKAα/ERK/CREB/BDNF signal was the main contributor to neuronal plasticity (Figure 8).

As a natural acetylcholinesterase inhibitor, HuA was demonstrated to improve LTP and synapse disfunction in AD animal models,[49] and elevated the expression of PSD95 in CIH mice.[16] HuA also restored cortico-hippocampal dysfunction connectivity in animals with a lesion of the nucleus basalis of Meynert (NBM).[50] HuA has an antidepressant-like effect in cognitive impairments and could improve neurological and cognitive functions via increasing p-CREB/CREB and BDNF levels in post-stroke depression rat.[51] Similarly, we found improved PSD structure, synaptic spine density, and PKAα/ERK/CREB/BDNF signal after treatment with HuA-LIP in CIH mice.

An abundance of evidence suggests that iron overload has a close relationship with neuronal injury. Accumulated iron could exacerbate neurotoxicity through oxidative processes, which has been demonstrated in neurodegenerative disease[19,52] and ischemic stroke.[17,27] Meanwhile, an excess of iron may direct neurotoxicity, especially in neurons vulnerable to toxic insults.[4] A previous study has reported that excessive iron treatment directly leads to LTP by an electrophysiological approach.[53] Intrahippocampal iron causes toxic effects and cognitive dysfunction manifested by the damage of dendritic structure and downregulation of synapse-related proteins, including BDNF, SYP, PSD95, and tenascin C.[54] At the same time, excess iron could accelerate mitochondrial oxidative damage caused by CIH.[16,34]

HuA was proven to be a neuroprotective effect via a non-cholinergic mechanism, targeting iron homeostasis and oxidative stress.[22,23,55] As similarly to iron chelator, HuA could reduce the capacity of iron regulatory protein-1 (IRP-1) binding to iron-responsive element (IRE) in APP promoter and inhibit APP translation in AD model.[23] The transferrin-bound iron (TBI), namely the Tf-TfR1 complex, is the main pathway of iron intake in CNS.[19] HuA were reported to reduce iron levels via declining TfR1 levels in AD[22,23] and CIH[16] models. Molecular docking molecular dynamics simulation demonstrated HuA could bind with the functionally active region of Tf, providing a direct reason for reducing TBI-depended iron uptake in CNS diseases.[56] In this study, we found that HuA-LIP decreased ferric content and the total iron content, which was superior to solely HuA administration. However, HuA cannot chemically react directly with ferrous and ferric iron (Figure 7). The decline of TfR1 and FTL, and increased FPN1 treated with HuA-LIP in CIH mice suggests that HuA-LIP protects neurons against CIH by modulating iron homeostasis and iron distribution (Figure 9). Of course, systematic regulation of iron metabolism via hepcidin-FPN1 was not excluded.

The biosafety of nanocontainer systems, when applied in vivo, should be paid more considerable attention, especially in some chronic diseases with long-term drug treatment. The class of quantum dots nanostructures is currently constituted by heavy elements which could cause the threat to the fertility and gestation of female mice.[57] Study also revealed that nanoscale graphene oxide (NGO) injected concentrations ≥ 200 μg/mL or 8

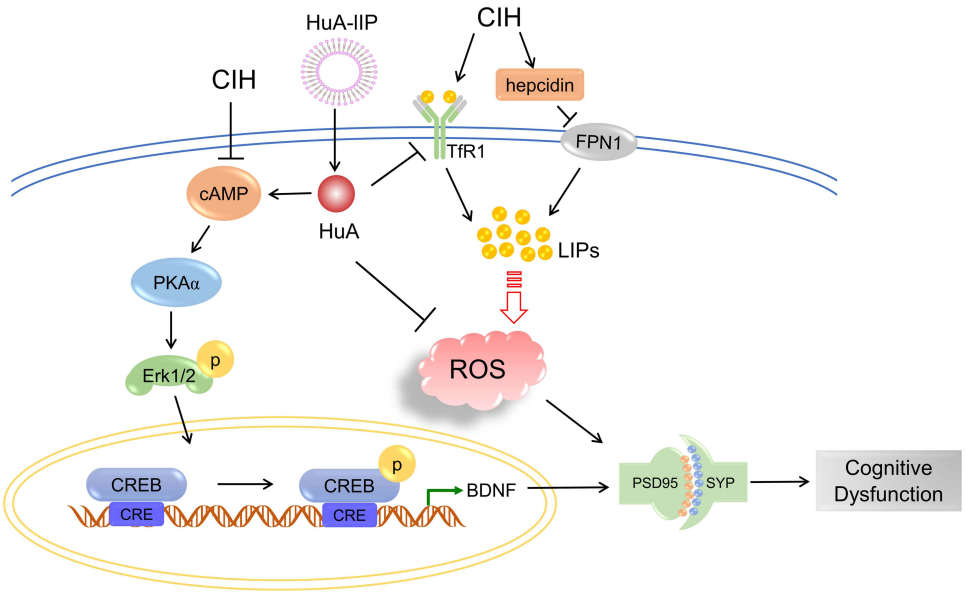

Figure 9 A schematic representation of the proposed neuroprotective mechanism of Huperzine-Liposome after CIH exposure. Once HuA-LIP is transported into cells, HuA is released. On the one hand, HuA activated PKAα/Erk/CREB/BDNF signaling pathway to improve synaptic disfunction. On the other hand, HuA inhibited the elevated TfR1, hepcidin and FTL expression to decrease excessive iron and oxidative damage.

weeks could harm the spermatogenesis and reproductive ability of mice.[58] Our previous study found no noticeable morphological changes in the brain, lung epithelial cells, and tracheal mucosa after nasal delivery of nanoliposome-encapsulated ferric ammonium citrate.[28] In our study, we did not find an adverse effect of HuA-LIP on the treatment CIH mice for 21 days. However, we should focus on the dose and timing of HuA administration on our further study.

Conclusions

In summary, we prepared of HuA-LIP and revealed the therapeutic effects on neural injury induced by CIH exposure. HuA-LIP had a good stability and controlled release. The potential neuroprotective mechanism of HuA-LIP manifested by improving neuronal damage, synaptic plasticity and cognitive disfunction owing to the ability to suppress iron overload and oxidative stress (Figure 9).

Author Contributions

Conceptualization and study design: Yashuo Zhao, En-Sheng Ji, Xin-Yue Yang, Li-Na Geng. Execution: Xin-Yue Yang, Ronghui Li, Ji-Xian Song, Cui-Ling Jia, Shan Xu, Ya-Jing Guo. Acquisition of data, analysis and interpretation: Xin-Yue Yang, Li-Na Geng, Yashuo Zhao, Cui-Ling Jia, Ji-Ren An, Meng-Fan Sun. Writing of original draft and visualization: Yashuo Zhao, En-Sheng Ji, Xin-Yue Yang, Li-Na Geng. Funding acquisition: Yashuo Zhao and En-Sheng Ji.

Funding

This work was supported by the National Natural Science Foundation of China [grant number, 82004127], Natural Science Foundation of Hebei [grant number, C2019423117 and H2022423352] and Funded by Science and Technology Project of Hebei Education Department [grant number, ZD2022013].

Disclosure

No potential conflict of interest was reported by the author(s).

References

1. Andrade AG, Bubu OM, Varga AW, et al. The relationship between obstructive sleep apnea and Alzheimer's disease. *J Alzheimers Dis*. 2018;64 (s1):S255–S270. doi:10.3233/JAD-179936
2. Xu L, Li Q, Ke Y, et al. Chronic intermittent hypoxia-induced aberrant neural activities in the hippocampus of male rats revealed by long-term in vivo recording. *Front Cell Neurosci*. 2021;15:784045. doi:10.3389/fncel.2021.784045
3. Gagnon K, Baril -A-A, Gagnon J-F, et al. Cognitive impairment in obstructive sleep apnea. *Pathol Biol*. 2014;62(5):233–240. doi:10.1016/j.patbio.2014.05.015
4. Zhao YS, Tan M, Song J-X, et al. Involvement of hepcidin in cognitive damage induced by chronic intermittent hypoxia in mice. *Oxid Med Cell Longev*. 2021;2021:8520967. doi:10.1155/2021/8520967
5. Benjafield AV, Ayas NT, Eastwood PR, et al. Estimation of the global prevalence and burden of obstructive sleep apnoea: a literature-based analysis. *Lancet Respir Med*. 2019;7(8):687–698. doi:10.1016/S2213-2600(19)30198-5
6. Lee W, Nagubadi S, Kryger MH, et al. Epidemiology of obstructive sleep apnea: a population-based perspective. *Expert Rev Respir Med*. 2008;2 (3):349–364. doi:10.1586/17476348.2.3.349
7. Rosenzweig I, Glasser M, Polsek D, et al. Sleep apnoea and the brain: a complex relationship. *Lancet Respir Med*. 2015;3(5):404–414. doi:10.1016/S2213-2600(15)00090-9
8. Xu LH, Xie H, Shi Z-H, et al. Critical role of endoplasmic reticulum stress in chronic intermittent hypoxia-induced deficits in synaptic plasticity and long-term memory. *Antioxid Redox Signal*. 2015;23(9):695–710. doi:10.1089/ars.2014.6122
9. Khuu MA, Pagan CM, Nallamothu T, et al. Intermittent hypoxia disrupts adult neurogenesis and synaptic plasticity in the dentate gyrus. *J Neurosci*. 2019;39(7):1320–1331. doi:10.1523/JNEUROSCI.1359-18.2018
10. Shiota S, Takekawa H, Matsumoto S-E, et al. Chronic intermittent hypoxia/reoxygenation facilitate amyloid-beta generation in mice. *J Alzheimers Dis*. 2013;37(2):325–333. doi:10.3233/JAD-130419
11. Marciante AB, Howard J, Kelly MN, et al. Dose-dependent phosphorylation of endogenous Tau by intermittent hypoxia in rat brain. *J Appl Physiol*. 2022;133(3):561–571. doi:10.1152/japplphysiol.00332.2022
12. Kazim SF, Sharma A, Saroja SR, et al. Chronic intermittent hypoxia enhances pathological tau seeding, propagation, and accumulation and exacerbates Alzheimer-like memory and synaptic plasticity deficits and molecular signatures. *Biol Psychiatry*. 2022;91(4):346–358. doi:10.1016/j.biopsych.2021.02.973
13. Wang J, Xu Z, Xu L, et al. Inhibition of STAT3 signal pathway recovers postsynaptic plasticity to improve cognitive impairment caused by chronic intermittent hypoxia. *Sleep Breath*. 2022. doi:10.1007/s11325-022-02671-6
14. Wall AM, Corcoran AE, O'Halloran KD, et al. Effects of prolyl-hydroxylase inhibition and chronic intermittent hypoxia on synaptic transmission and plasticity in the rat CA1 and dentate gyrus. *Neurobiol Dis*. 2014;62:8–17. doi:10.1016/j.nbd.2013.08.016
15. Zhao YS, An J-R, Yang S, et al. Hydrogen and oxygen mixture to improve cardiac dysfunction and myocardial pathological changes induced by intermittent hypoxia in rats. *Oxid Med Cell Longev*. 2019;2019:7415212. doi:10.1155/2019/7415212
16. An JR, Zhao Y-S, Luo L-F, et al. Huperzine A, reduces brain iron overload and alleviates cognitive deficit in mice exposed to chronic intermittent hypoxia. *Life Sci*. 2020;250:117573. doi:10.1016/j.lfs.2020.117573
17. Wang P, Cui Y, Ren Q, et al. Mitochondrial ferritin attenuates cerebral ischaemia/reperfusion injury by inhibiting ferroptosis. *Cell Death Dis*. 2021;12(5):447. doi:10.1038/s41419-021-03725-5
18. You L, Yu -P-P, Dong T, et al. Astrocyte-derived hepcidin controls iron traffic at the blood-brain-barrier via regulating ferroportin 1 of microvascular endothelial cells. *Cell Death Dis*. 2022;13(8):667. doi:10.1038/s41419-022-05043-w
19. You LH, Yan C-Z, Zheng B-J, et al. Astrocyte hepcidin is a key factor in LPS-induced neuronal apoptosis. *Cell Death Dis*. 2017;8(3):e2676. doi:10.1038/cddis.2017.93
20. Kwan P, Ho A, Baum L. Effects of deferasirox in Alzheimer's disease and tauopathy animal models. *Biomolecules*. 2022;12(3):365 doi:10.3390/biom12030365.
21. Zhang HY, Zheng CY, Yan H, et al. Potential therapeutic targets of huperzine A for Alzheimer's disease and vascular dementia. *Chem Biol Interact*. 2008;175(1–3):396–402. doi:10.1016/j.cbi.2008.04.049
22. Tao LX, Huang X-T, Chen Y-T, et al. Acetylcholinesterase-independent protective effects of huperzine A against iron overload-induced oxidative damage and aberrant iron metabolism signaling in rat cortical neurons. *Acta Pharmacol Sin*. 2016;37(11):1391–1400. doi:10.1038/aps.2016.78
23. Huang XT, Qian Z-M, He X, et al. Reducing iron in the brain: a novel pharmacologic mechanism of huperzine A in the treatment of Alzheimer's disease. *Neurobiol Aging*. 2014;35(5):1045–1054. doi:10.1016/j.neurobiolaging.2013.11.004
24. Zorkina Y, Abramova O, Ushakova V, et al. Nano carrier drug delivery systems for the treatment of neuropsychiatric disorders: advantages and limitations. *Molecules*. 2020;25(22):5294 doi:10.3390/molecules25225294.
25. Sun Y, Xie Y, Tang H, et al. In vitro and in vivo evaluation of a novel estrogen-targeted PEGylated oxaliplatin liposome for gastric cancer. *Int J Nanomedicine*. 2021;16:8279–8303. doi:10.2147/IJN.S340180
26. Zhao Y-Z, Lin M, Lin Q, et al. Intranasal delivery of bFGF with nanoliposomes enhances in vivo neuroprotection and neural injury recovery in a rodent stroke model. *J Control Release*. 2016;224:165–175. doi:10.1016/j.jconrel.2016.01.017
27. Zhao Y, Xin Z, Li N, et al. Nano-liposomes of lycopene reduces ischemic brain damage in rodents by regulating iron metabolism. *Free Radic Biol Med*. 2018;124:1–11. doi:10.1016/j.freeradbiomed.2018.05.082
28. Guo X, Zheng H, Guo Y, et al. Nasal delivery of nanoliposome-encapsulated ferric ammonium citrate can increase the iron content of rat brain. *J Nanobiotechnology*. 2017;15(1):42. doi:10.1186/s12951-017-0277-2
29. Kong D, Hong W, Yu M, et al. Multifunctional targeting liposomes of epirubicin plus resveratrol improved therapeutic effect on brain gliomas. *Int J Nanomedicine*. 2022;17:1087–1110. doi:10.2147/IJN.S346948
30. Amani H, Habibey R, Hajmiresmail SJ, et al. Antioxidant nanomaterials in advanced diagnoses and treatments of ischemia reperfusion injuries. *J Mater Chem B*. 2017;5(48):9452–9476. doi:10.1039/C7TB01689A
31. Afshari R, Akhavan O, Hamblin MR, et al. Review of oxygenation with nanobubbles: possible treatment for hypoxic COVID-19 patients. *ACS Appl Nano Mater*. 2021;4(11):11386–11412. doi:10.1021/acsanm.1c01907

32. Wang S, Li W, Sun K, et al. Study of release kinetics and degradation thermodynamics of ferric citrate liposomes. *Chem Phys Lipids*. 2019;225:104811. doi:10.1016/j.chemphyslip.2019.104811
33. Xiao X, Chen Q, Zhu X, et al. ABAD/17β-HSD10 reduction contributes to the protective mechanism of huperzine a on the cerebral mitochondrial function in APP/PS1 mice. *Neurobiol Aging*. 2019;81:77–87. doi:10.1016/j.neurobiolaging.2019.05.016
34. Song JX, Zhao Y-S, Zhen Y-Q, et al. Banxia-Houpu decoction diminishes iron toxicity damage in heart induced by chronic intermittent hypoxia. *Pharm Biol*. 2022;60(1):609–620. doi:10.1080/13880209.2022.2043392
35. Kandzija N, Khutoryanskiy VV. Delivery of riboflavin-5'-monophosphate into the cornea: can liposomes provide any enhancement effects? *J Pharm Sci*. 2017;106(10):3041–3049. doi:10.1016/j.xphs.2017.05.022
36. Yan Q, Wang W, Weng J, et al. Dissolving microneedles for transdermal delivery of huperzine A for the treatment of Alzheimer's disease. *Drug Deliv*. 2020;27(1):1147–1155. doi:10.1080/10717544.2020.1797240
37. Li F, Hu R, Wang B, et al. Self-microemulsifying drug delivery system for improving the bioavailability of huperzine A by lymphatic uptake. *Acta Pharm Sin B*. 2017;7(3):353–360. doi:10.1016/j.apsb.2017.02.002
38. Jiang Y, Liu C, Zhai W, et al. The optimization design of lactoferrin loaded Hupa nanoemulsion for targeted drug transport via intranasal route. *Int J Nanomedicine*. 2019;14:9217–9234. doi:10.2147/IJN.S214657
39. Huang Q, Wang P, Liu H, et al. Inhibition of ERK1/2 regulates cognitive function by decreasing expression levels of PSD-95 in the hippocampus of CIH rats. *Eur J Neurosci*. 2022;55(6):1471–1482. doi:10.1111/ejn.15635
40. Cho KO, Hunt CA, Kennedy MB. The rat brain postsynaptic density fraction contains a homolog of the Drosophila discs-large tumor suppressor protein. *Neuron*. 1992;9(5):929–942. doi:10.1016/0896-6273(92)90245-9
41. Tian M, Stroebel D, Piot L, et al. GluN2A and GluN2B NMDA receptors use distinct allosteric routes. *Nat Commun*. 2021;12(1):4709. doi:10.1038/s41467-021-25058-9
42. Yan L, Jin Y, Pan J, et al. 7,8-dihydroxycoumarin alleviates synaptic loss by activated PI3K-Akt-CREB-BDNF signaling in Alzheimer's disease model mice. *J Agric Food Chem*. 2022;70(23):7130–7138. doi:10.1021/acs.jafc.2c02140
43. Lu Y, Christian K, Lu B. BDNF: a key regulator for protein synthesis-dependent LTP and long-term memory? *Neurobiol Learn Mem*. 2008;89(3):312–323. doi:10.1016/j.nlm.2007.08.018
44. Xie H, Leung K-L, Chen L, et al. Brain-derived neurotrophic factor rescues and prevents chronic intermittent hypoxia-induced impairment of hippocampal long-term synaptic plasticity. *Neurobiol Dis*. 2010;40(1):155–162. doi:10.1016/j.nbd.2010.05.020
45. Flores KR, Viccaro F, Aquilini M, et al. Protective role of brain derived neurotrophic factor (BDNF) in obstructive sleep apnea syndrome (OSAS) patients. *PLoS One*. 2020;15(1):e0227834. doi:10.1371/journal.pone.0227834
46. Xu W, Yao X, Zhao F, et al. Changes in hippocampal plasticity in depression and therapeutic approaches influencing these changes. *Neural Plast*. 2020;2020:8861903. doi:10.1155/2020/8861903
47. Li L, Yang Y, Zhang H, et al. Salidroside ameliorated intermittent hypoxia-aggravated endothelial barrier disruption and atherosclerosis the cAMP/PKA/RhoA signaling pathway. *Front Pharmacol*. 2021;12:723922. doi:10.3389/fphar.2021.723922
48. Fei E, Xiong WC, Mei L. Ephrin-B3 recruits PSD-95 to synapses. *Nat Neurosci*. 2015;18(11):1535–1537. doi:10.1038/nn.4147
49. Wang K, Sun W, Zhang L, et al. Oleanolic acid ameliorates abeta 25-35 Injection-induced memory deficit in Alzheimer's disease model rats by maintaining synaptic plasticity. *CNS Neurol Disord Drug Targets*. 2018;17(5):389–399. doi:10.2174/1871527317666180525113109
50. Rispoli V, Ragusa S, Nisticò R, et al. Huperzine a restores cortico-hippocampal functional connectivity after bilateral AMPA lesion of the nucleus basalis of meynert. *J Alzheimers Dis*. 2013;35(4):833–846. doi:10.3233/JAD-130278
51. Du Y, Liang H, Zhang L, et al. Administration of Huperzine A exerts antidepressant-like activity in a rat model of post-stroke depression. *Pharmacol Biochem Behav*. 2017;158:32–38. doi:10.1016/j.pbb.2017.06.002
52. Zhao YS, Zhang L-H, Yu -P-P, et al. Ceruloplasmin, a potential therapeutic agent for Alzheimer's disease. *Antioxid Redox Signal*. 2018;28(14):1323–1337. doi:10.1089/ars.2016.6883
53. De la fuente-ortega E, Plaza-Briceño W, Vargas-Robert S, et al. Prenatal Ethanol Exposure Misregulates Genes Involved in Iron Homeostasis Promoting a Maladaptation of Iron Dependent Hippocampal Synaptic Transmission and Plasticity. *Front Pharmacol*. 2019;10:1312. doi:10.3389/fphar.2019.01312
54. Zhang Y, Bai X, Zhang Y, et al. Hippocampal Iron accumulation impairs synapses and memory via suppressing furin expression and down-regulating BDNF Maturation. *Mol Neurobiol*. 2022;59(9):5574–5590. doi:10.1007/s12035-022-02929-w
55. Friedli MJ, Inestrosa NC. Huperzine A and its neuroprotective molecular signaling in Alzheimer's disease. *Molecules*. 2021;26(21):6531. doi:10.3390/molecules26216531
56. Atiya A, Alhumaydhi FA, Shamsi A, et al. Mechanistic insight into the binding of huperzine a with human transferrin: computational, spectroscopic and calorimetric approaches. *ACS Omega*. 2022;7(43):38361–38370. doi:10.1021/acsomega.2c03185
57. Akhavan O, Hashemi E, Zare H, et al. Influence of heavy nanocrystals on spermatozoa and fertility of mammals. *Mater Sci Eng C Mater Biol Appl*. 2016;69:52–59. doi:10.1016/j.msec.2016.06.055
58. Akhavan O, Ghaderi E, Hashemi E, Akbari E. Dose-dependent effects of nanoscale graphene oxide on reproduction capability of mammals. *Carbon*. 2015;95:309–317. doi:10.1016/j.carbon.2015.08.017